BIOCHEMISTRY
including biophysical chemistry & molecular biology

Article

pubs.acs.org/biochemistry

Independent Interactions of Ubiquitin-Binding Domains in a Ubiquitin-Mediated Ternary Complex

Thomas P. Garner,[†] Joanna Strachan,[‡] Elizabeth C. Shedden,[†] Jed E. Long,[†] James R. Cavey,[‡] Barry Shaw,[‡] Robert Layfield,[‡] and Mark S. Searle*,[†]

[†]Centre for Biomolecular Sciences, School of Chemistry, University Park, University of Nottingham, Nottingham NG7 2RD, U.K.
[‡]School of Biomedical Sciences, Queen's Medical Centre, University of Nottingham, Nottingham NG7 2UH, U.K.

Supporting Information

ABSTRACT: Ubiquitin (Ub) modifications are transduced by receptor proteins that use Ub-binding domains (UBDs) to recognize distinct interaction faces on the Ub surface. We report the nuclear magnetic resonance (NMR) solution structures of the A20-like zinc finger (A20 Znf) UBD of the Ub receptor ZNF216, and its complex with Ub, and show that the binding surface on Ub centered on Asp58 leaves the canonical hydrophobic Ile44 patch free to participate in additional interactions. We have modeled ternary complexes of the different families of UBDs and show that while many are expected to bind competitively to the same Ile44 surface or show steric incompatibility, other combinations (in particular, those involving the A20 Znf domain) are consistent with a single Ub moiety simultaneously participating in multiple interactions with different UBDs. We subsequently demonstrate by NMR that the A20 Znf domain of ZNF216 and the UBA domain of the p62 protein (an Ile44-binding UBD), which function in the same biological pathways, are able to form such a Ub-mediated ternary complex through independent interactions with a single Ub. This work supports an emerging concept of Ub acting as a scaffold to mediate multiprotein complex assembly.

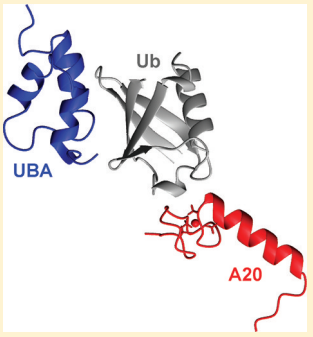

Reversible post-translational modification (PTM) of proteins is a fundamental mechanism by which cells respond to external and internal stimuli to control intracellular signaling events. Two principal PTMs are phosphorylation and ubiquitination,[1,2] both of which may facilitate conformational changes leading to allosteric regulation or modified interaction surfaces for specific recognition.[2,3] Ubiquitin (Ub) is a particularly versatile protein modifier because of its ability to be assembled into polymeric chains that have different lengths and conformational properties, as a result of the use of different isopeptide linkages. While ubiquitination has the potential to alter the chemical properties of the modified protein, its effects are more commonly mediated via interaction with receptors containing a host of different Ub-binding domains (UBDs) with different binding specificities, of which there are more than 20 known families.[1,4,5] The majority of UBDs interact with Ub using a hydrophobic patch on its β-sheet surface with a binding locus defined by Ile44. However, it is increasingly apparent that Ub has multiple potential binding surfaces, and recently, UBDs that bind to noncanonical sites, including the C-terminal di-Gly, a polar surface centered on Asp58,[4,5] and a hydrophobic patch centered on Leu8 rather than Ile44, have been identified.[6]

The existence of multiple potential binding surfaces on Ub,[7] as well as the large number of different UBDs used by Ub receptors, suggests the possibility of simultaneous colocalization of two or more UBDs from different (or even the same) receptors within the same signaling pathway, adding further potential complexity and specificity to the recognition of PTMs. The advantages are yet to be fully explored but could include regulation of deubiquitinase activity and the ability to shuttle ubiquitinated substrates along specific pathways such as trafficking between intracellular receptors or delivery to the proteasome or lysosome.[1,4,8] Two rigidly linked UBDs (an inverted UIM and A20 Znf domain) within a single molecule of nucleotide exchange factor Rabex-5 have been shown to engage different Ub molecules in close proximity to facilitate direct Ub recruitment and covalent ubiquitination, linked to intrinsic Rabex-5 Ub ligase activity.[9,10] In addition, in the complex between the AMSH zinc metalloprotease and Lys63-linked diUb, AMSH forms critical functional contacts simultaneously with both the Ile44 binding face and an Ile36-centered patch on a distal Ub in regulating specific cleavage of Lys63-linked polyubiquitin chains.[11]

An increased level of breakdown of proteins in skeletal muscle, which occurs during muscle atrophy, is characteristic of several clinical conditions, including hyperthyroidism, sepsis, cancer cachexia, and AIDS. Genes that are upregulated during and directly mediate muscle atrophy are termed "atrogenes" and encode several components of the Ub proteasome system (UPS), including the E3 ubiquitin ligases MAFbx/Atrogin-1 and MuRF-1, both of which have been extensively studied.[12−14] In addition, the comparatively less well characterized Ub receptor ZNF216 (also known as ZFAND5), a protein that contains both A20- and AN1-type zinc fingers, has also been

Received: July 22, 2011
Revised: September 15, 2011
Published: September 16, 2011

identified as an atrogene.[12] Although there are sequence homologies among the A20 Znf domains of ZNF216, the E3 Ub-ligase Rabex-5, and the dual-function E3/deubiquitinating enzyme A20, ZNF216 does not appear to be catalytically active with respect to Ub conjugation and deconjugation.[12] The precise function of the ZNF216 protein with respect to muscle atrophy is unclear, although it appears to play a critical role as a shuttle factor delivering ubiquitinated proteins to the 26S proteasome and in other cell types has been shown to act as a regulator of NF-κB activity.[12,15,16] Indeed, the pathways that control NF-κB activation are regulated at multiple points by ubiquitination events, and many of the proteins linked to NF-κB regulation contain UBDs.[17] Several other Ub receptor proteins have been proposed to share the proteasome shuttle function with ZNF216, binding both ubiquitinated proteins and the proteasome, including p62/SQSTM1, which contains a C-terminal Ub-associated (UBA) domain that binds to the canonical Ile44-centered surface. Notably, p62 also shares several common interaction partners linked to NF-κB regulation with ZNF216, including TRAF6 and RIP,[16,18−20] indicating that these proteins may function within the same complex.

We describe the NMR structure of the A20 Znf UBD from ZNF216 and its high-affinity complex with Ub that uses a polar binding patch centered on Asp58 rather than the classical β-sheet Ile44 hydrophobic surface recognized by many other UBDs. Moreover, we show that the A20 Znf domain of ZNF216 and the UBA domain of p62 are capable of independent binding interactions in forming a ternary complex with a single Ub. We evaluate *in silico* other UBD pairings that could bind simultaneously to Ub, highlighting the possibility of Ub behaving as a "hub" for the recruitment and colocalization of Ub receptors for the regulation of diverse intracellular molecular signaling events.

MATERIALS AND METHODS

Protein Expression and Purification. The full-length ZNF216 expression vector was generated by polymerase chain reaction (PCR) amplification from rat skeletal muscle cDNA, including a *Bam*HI site in the 5′ PCR primer and a *Xho*I site in the 3′ primer, and ligation into the pGEX-4T-1 plasmid (GE Healthcare); this permits expression of ZNF216 as a GST fusion. A premature stop codon was incorporated after ZNF216 residue 60 using QuikChange site-directed mutagenesis (Stratagene) to generate the A20 Znf construct. The ZNF216 Cys30Ala and Cys33Ala double mutant was also generated by site-directed mutagenesis. All constructs were verified by DNA sequencing. Both full-length ZNF216 and the A20 Znf domain were expressed in *Escherichia coli* strain C41(DE3) in Luria broth (Sigma). ^{15}N-labeled and ^{13}C- and ^{15}N-labeled proteins were expressed in M9 medium supplemented with 30 μM $ZnCl_2$ containing $^{15}NH_4Cl$ (1 g/L) and [^{13}C]glucose (2 g/L). Yields of labeled protein were typically 3−4 mg/L compared with 4−6 mg/L for unlabeled protein produced from rich LB growth medium.

Overexpression was induced at an OD_{600} of 0.6 with 0.35 mM IPTG, and cells were grown at 20 °C for 18−20 h before being harvested and frozen at −80 °C. Cells containing unlabeled or isotopicaly labeled protein were resuspended in 10 mM Tris-HCl (pH 7.4), 150 mM NaCl, 50 μM $ZnCl_2$, 2 mM DTT, and 0.1% Triton X-100 in the presence of DNase1 at 0.2 mg/mL (Sigma) and Complete EDTA free protease inhibitor (Roche) and subjected to one 20 min freeze−thaw cycle at −80 °C before being lysed by sonication and centrifugation to isolate the soluble component. GST−ZNF216 and GST−A20 Znf fusion proteins were purified using 1 mL of glutathione Sepharose 4B (GE Healthcare) in a gravity flow column followed by an on column cleavage using 5 units of thrombin in 1 mL of 20 mM Tris-HCl (pH 8.4), 200 mM NaCl, 2.5 mM $CaCl_2$, and 50 μM $ZnCl_2$ for 16 h at 4 °C. Cleaved ZNF216 was diluted 4-fold before being loaded onto a HiTrap Q HP anionic exchange column (GE Healthcare) in 10 mM Tris-HCl (pH 7), 2 mM DTT, and 50 mM ZnCl and eluted using 250−450 mM NaCl. The pure protein was concentrated or buffer exchanged where appropriate using a spin concentrator and the protein concentration determined using the absorbance at 280 nm using a NanoDrop ND-100 spectrophotometer.

Cleaved A20 Znf protein was purified using a HiPrep Sephacryl S-100 gel filtration column (GE Healthcare) in 10 mM Tris-HCl, 150 mM NaCl, 2 mM DTT, and 50 μM $ZnCl_2$ followed by desalting using a 5 × 5 mL HiTrap desalting column (GE Healthcare) and freeze-dried. The purity and quality of all proteins were assessed using electrospray ionization mass spectrometry (ESI-MS) and shown to be >99% pure and of the expected mass. The expression and purification of the p62 UBA domain (residues 387−436) and Ub, both unlabeled and fully labeled with ^{13}C and ^{15}N, have been described previously.[18,21]

The Ub Lys48Cys mutant was generated by site-directed PCR using the QuikChange protocol (Stratagene). The paramagnetic spin-label *S*-(2,2,5,5-tetramethyl-2,5-dihydro-1*H*-pyrrol-3-yl)methyl methanesulfonothioate (MTSL) (Toronto Research Chemicals Inc.) was coupled to the single incorporated cysteine as described previously.[22] More than 95% coupling was confirmed by ESI-MS. Paramagnetic MTSL was reduced over a period of 12 h with a 5-fold molar excess of buffered sodium ascorbate.

Biochemical Binding Studies. Thrombin-cleaved ZNF216 (wild type and mutant) was immobilized using cyanogen bromide-activated Sepharose 4B (GE Healthcare) (~250 μg of protein on 50 μL of beads) and used to capture ubiquitinated proteins from U20S cells from 3 × 75 cm^3 tissue culture flasks at confluency. Cells were sonicated in 8 mL of 50 mM Tris-HCl (pH 7.5), 150 mM NaCl, 0.5% NP-40, 5 mM NEM, 0.1% mammalian protease inhibitor cocktail (Sigma), and 20 μM MG132 (ENZO). After centrifugation, DTT was added to a final concentration of 10 mM, and proteins were bound to immobilized ZNF216 (6 mg of total protein per 50 μL of ZNF216 beads) overnight at 4 °C with mixing. Unbound proteins were removed by being washed with 50 mM Tris-HCl (pH 7.5), 150 mM NaCl, 0.5% NP-40, and 1 mM DTT. Bound proteins were eluted from the beads with gel loading buffer and detected by western blotting with p62 [mouse monoclonal anti-p62 lck ligand (BD Biosciences)] or Ub [rabbit anti-Ub (in house)] antibodies. "Load" represents 1.25% of the cell lysate loaded onto the beads, and 50% of the total ZNF216-bound proteins was analyzed on each blot. For membrane-based binding assays, purified Ub with the indicated mutations (ENZO) was spotted onto nitrocellulose that after blocking was incubated with bacterial lysates containing GST−ZNF216 proteins (equivalent to 1 mL of overexpression culture per membrane), for 2 h at 4 °C. Bound GST−ZNF216 protein was detected by western blotting (anti-GST) (Bethyl) and Ub by anti-Ub (in house).

Cell Transfection, Indirect Immunofluorescence Staining, and Confocal Microscopy. Human U20S (osteosarco-

ma-derived) cells were transfected with LT1 (GeneFlow) according to the manufacturer's instructions, using 0.5 μg of total plasmid DNA per well in 12-well plates. All wells were transfected with 125 ng each of untagged wt-p62, FLAG-TRAF6, and His-Tyg-Ub (All pcDNA3.1). Wells were additionally transfected with 125 ng of pcDNA3.1 empty vector, Xpress-wt-ZNF216, or Xpress-mut-ZNF216. Cells were washed with sterile phosphate-buffered saline (PBS) 24 h post-transfection and fixed in 4% (w/v) paraformaldehyde for 10 min. Cells were washed with PBS (3 × 5 min) prior to permeabilization with 0.1% (v/v) Triton X-100 in PBS for 15 min. Cells were then blocked [0.5% (w/v) fish skin gelatin, 0.2% (w/v) BSA in PBS] for 30 min. Coverslips were washed in PBS and then incubated in 1:1000 mouse monoclonal anti-Xpress (Invitrogen) or 1:1000 rabbit polyclonal anti-p62 (ENZO) in PBS for 1 h. Cells were washed with PBS and then incubated with Alexafluor 488 anti-mouse IgG and Alexafluor 568 goat anti-rabbit IgG (Invitrogen), both at a 1:1000 dilution in PBS, for 1 h. After being washed with PBS, cells were incubated in a 1:20000 dilution of Hoescht 33258 for 5 min before a final 2 × 5 min wash in PBS. Coverslips were mounted on slides and imaged with a Leica TCS SP2 laser scanning confocal microscope.

Sequence Alignment and Bioinformatics. The sequences of A20 Znf domains were selected using the UniProt search tool. Sequence alignment was performed on the full-length proteins and on the A20 Znf sequences alone in ClustalX 2.0.11.[23,24] The sequence for the ZNF216 protein was subjected to analysis using SMART, PROSCAN, and ELM to search for potential domains or functional motifs and the DisProt server (http://www.disprot.org) used to identify intrinsically disordered regions.[25,26]

NMR Spectroscopy. NMR data were collected at 600 MHz on a Bruker Avance spectrometer fitted with a TXI triple-resonance probe with a *z*-axis gradient using standard pulse sequences. The NMR assignment of the unbound A20 Znf domain was achieved using 1 mM unlabeled and ^{15}N-labeled protein and 0.7 mM ^{13}C- and ^{15}N-labeled protein samples in 5 mM Tris-HCl (pH 7), 50 mM NaCl, 2 mM tris(2-carboxyethyl)phosphine (TCEP), 50 μM $ZnCl_2$, 10% D_2O, and 0.04% sodium azide at 298 K. Assignment was achieved using the standard methodology using ^{1}H−^{1}H NOESY (mixing times of 100, 150, and 250 ms), ^{1}H−^{1}H TOCSY, ^{15}N HSQC, ^{13}C HSQC, HNCO, HN(CA)CO, CBCANH, CBCA(CO)-NH, HCCH-TOCSY, ^{13}C HSQC-NOESY (mixing time of 150 ms), ^{15}N HSQC-TOCSY, and ^{15}N HSQC-NOESY (mixing time of 150 ms). Spectra were processed using Topspin version 2.1 (Bruker), and assignments were made in CCPNMR.[27]

Backbone $^1D_{NH}$ residual dipolar couplings were obtained from the difference in ^1J scalar couplings measured from ^{1}H−^{15}N IPAP-HSQC spectra for both free and Ub-bound ^{15}N-labeled A20 Znf and A20 Znf bound ^{15}N-labeled Ub.[28] The solutions were soaked into predried 6 mm 5 and 7% polyacrylamide gels, which were then compressed into a 5 mm NMR tube (Worldwide Glass Resource Ltd., Cambridge, U.K.).[29] ^{1}H−^{15}N heteronuclear NOEs were recorded on a 1 mM [^{15}N]A20 Znf domain sample in the absence of Ub, in the presence of 2 mM Ub, and in the presence of 2 mM Ub and 4 mM p62-UBA.[30] ^{13}C/^{15}N half-filtered experiments were conducted with 1 mM [^{13}C−^{15}N]Ub mixed with 1.5 mM unlabeled A20 Znf domain following the method of Otting *et al.* with 416 scans and a mixing time of 250 ms.[31]

Paramagnetic relaxation enhancement ^{15}N HSQC spectra were recorded with a 5 s relaxation delay on both paramagnetic and diamagnetic complexes of 1 mM [^{15}N]A20 Znf with 2 mM Ub-K48C-MTSL. Paramagnetic relaxation enhancement (PRE) and distance restraints were calculated as described in previous studies.[22,32,33]

NMR Binding Studies. Unlabeled protein was added in a stepwise manner to a 1 mM sample of ^{15}N-labeled partner protein up to a 4:1 ratio. Data were collected on both ^{15}N-labeled Ub and ^{15}N-labeled A20 Znf at 298 K, and changes in chemical shifts and cross-peak intensities were monitored by acquisition of ^{1}H−^{15}N HSQC spectra. For studying the formation of a ternary complex on Ub, a 1 mM [^{15}N]Ub sample was first saturated with 2 mM A20 Znf before the stepwise addition of up to 4 mM p62 UBA at 298 K. Changes in chemical shifts and cross-peak intensities were monitored by acquisition of HSQC spectra. This was repeated using [^{15}N]A20 Znf and also [^{15}N]p62 UBA saturated with Ub before addition of the second binding partner. Chemical shift perturbations (CSPs) were calculated as $\Delta\delta_{HSQC} = [(\Delta\delta_H)^2 + (\Delta\delta_N/5)^2]^{1/2}$, where $\Delta\delta_H$ and $\Delta\delta_N$ are the observed shifts in the ^{1}H and ^{15}N dimensions of the HSQC spectrum, respectively.

A20 Znf Domain Structure Calculations. The structure was determined on the basis of 446 NOE distance restraints derived from the ^{1}H−^{1}H NOESY, ^{1}H−^{13}C HSQC-NOESY, and ^{1}H−^{15}N HSQC-NOESY spectra and 177 dihedral restraints predicted from NMR chemical shifts using PREDITOR.[34] The NOEs were classified on the basis of their intensity into strong (1.8−2.8 Å), medium (1.8−4 Å), weak (1.8−5 Å), and very weak (1.8−6 Å) classes. In addition, 30 backbone $^1D_{NH}$ RDC parameters were used as restraints using the ISAC method and visualized using MODULE.[35,36] An initial 200 structures were produced using the standard three-step XPLOR-NIH 2.14 protocol.[37] In the first stage, high-temperature Cartesian dynamics was performed at 1000 K with a time step of 0.005 ps, for 20000 steps, using the Verlet integrator. During the second cooling phase of the protocol, the temperature was reduced from 1000 to 100 K in steps of 50 K, with a time step of 5 fs, over 40000 steps during which the relative weighting of nonbonded energy terms was increased from 10% of their default values to their force field default.[38,39] These initial structures were then refined with another 10000 cooling steps. The 20 lowest-energy structures were selected on the basis of small NOE and dihedral angle violations of less than ±0.2 Å and ±5°, respectively. All structures were analyzed statistically using the protein structure validation software suite (see Table 1)[40] and displayed using MOLMOL.[41] A compact core structure is evident for residues 12−42; however, much poorer structural definition is evident within the N- and C-termini. Heteronuclear ^{15}N(^{1}H) NOEs, a good indicator of local dynamics, show an average NOE value of 0.65 for residues 12−42 that decreases rapidly at the N- and C-termini, becoming large and negative. In addition, measured chemical shift indices, the low number of restraints per residue, and RDC values that average close to zero are consistent with the intrinsic flexibility and disorder in the N- and C-termini.

The structure was refined for the A20 Znf domain in the bound state using 345 NOE distance restraints from ^{1}H−^{15}N HSQC-NOESY and ^{13}C and ^{15}N half-filtered NOESY experiments, 30 $^1D_{NH}$ RDC restraints, and 161 dihedral angle restraints predicted from backbone chemical shifts. The XPLOR-NIH protocol was again used but with the unbound

Table 1. NMR and Refinement Statistics for the A20 Znf Domain of ZNF216

NMR distance and dihedral constraints	
total no. NOE distance restraints	446
intraresidue	54
inter-residue	392
sequential ($\|i - j\| = 1$)	152
medium-range ($\|i - j\| < 4$)	108
long-range ($\|i - j\| > 5$)	132
hydrogen bond	0
total no. of dihedral angle restraints	177
ϕ	57
ψ	48
total no. of RDC restraints	30
structure statistics	
violations (mean and standard deviation)	
distance constraints (Å)	0.02
dihedral angle constraints (deg)	0.46
maximal dihedral angle violation (deg)	4.6
maximal distance constraint violation (Å)	0.2
deviations from idealized geometry	
bond lengths (Å)	0.011
bond angles (deg)	1.4
impropers (deg)	0.41
average pairwise rmsd[a] (Å)	
heavy	0.9
backbone	0.3
structure quality factors	
Procheck *G* factor (ϕ and ψ only)	−0.15
Procheck *G* factor (all dihedral angles)	−0.13
Verify3D	0.24
MolProbity clash score	3.11
Ramachandran statistics[a] (Procheck/MolProbity)	
favored (%)	81.7/88.7
additionally allowed (%)	18.3/10.9
generously allowed (%)	0/NA
disallowed (%)	0/0.3

[a]Pairwise rmsd and Ramachandran statistics were calculated among 20 refined structures for the ordered region of the structure defined by residues 12−42, with a total of 18 restraints per residue.

A20 structure as the starting point. The 10 lowest-energy A20 Znf domain structures were selected (pairwise backbone rmsd of 0.6 Å and rmsd of 0.7 Å for the unbound ensemble of structures). Generation of the structure of the complex was performed with structures calculated for both the free and bound A20 Znf with little difference in the final structures. A combination of CSP mapping (including mutation-induced effects), NOE and PRE restraints, and RDC restraints was used to generate a family of structures with a chemical shift refined[42] yeast Ub homology model to form a binary complex with the A20 Znf domain using HADDOCK.[43] The disordered N- and C-terminal "tail" of the A20 Znf domain and the C-terminal tail of Ub were removed as part of the docking protocol.[43] The electrostatic energy terms were disabled during the flexible docking protocol but included the "ZN ion" patch. Initial modeling identified close contacts between Asp58 of Ub and Ser31 of A20 Znf, as also observed for the Rabex-5 structure, and consistent with CSPs for the NH group of Ser31 of ∼1.5 ppm. In light of the experimental data, hydrogen bonding restraints were used in the HADDOCK refinement. A total of 500 structures were generated from the rigid body docking protocol; 50 of those were selected for further "semiflexible" and "fully flexible" docking refinement. Forty of the 50 structures showed no distance violations and violated less than 10% of the intervector projection angle restraints. The 40 structures clustered into the same HADDOCK-defined cluster with a 1.5 Å cutoff value. Finally, 10 of the 40 structures with the lowest HADDOCK energies were selected to represent the structural ensemble giving a HADDOCK energy of −35 ± 1.5 kcal/mol and a pairwise rmsd of 0.5 Å across all residues. The ensemble was analyzed statistically as described above using the protein structure validation software suite (see Table 2).[40] Hydrophobic surface area measurements were performed using Naccess (version 2.1.1).[44]

Table 2. NMR and Refinement Statistics for the Complex of the A20 Znf Domain with Ubiquitin

NMR distance and dihedral constraints	
total no. of intermolecular restraints	40
total no. of NOEs	4
total no. of PREs[a]	29
total no. of CSPs	4
hydrogen bond	3
total no. of dihedral angle restraints	0
total no. of RDC restraints[b]	102
structure statistics	
violations	
distance constraints (Å)	0.04
maximal distance constraint violation (Å)	0.5
dihedral angle constraints (deg)	NA
maximal dihedral angle violation (deg)	NA
deviations from idealized geometry	
bond lengths (Å)	0.011
bond angles (deg)	1.5
impropers (deg)	0.4
average pairwise rmsd[c] (Å)	
heavy	0.5
backbone	0.5
structure quality factors	
Procheck *G* factor (ϕ and ψ only)	−0.17
Procheck *G* factor (all dihedral angles)	−0.13
Verify3D	0.41
MolProbity clash score	13.66
Ramachandran statistics[d] (Procheck/MolProbity)	
favored (%)	88.7/94.3
additionally allowed (%)	11.3/5.7
generously allowed (%)	0/NA
disallowed (%)	0/1.3

[a]PRE, paramagnetic relaxation enhancement. [b]RDC restraints included 30 for the A20 domain and 72 for ubiquitin. [c]The pairwise rmsd was calculated among the 10 lowest-energy structures. [d]Ordered region of the structure define by residues 12−42.

Structural Modeling. The ternary complexes shown in Figures 3 and 4 were generated by manual docking of UBDs based on the coordinates of binary complexes deposited in the Protein Data Bank (PDB). Each structure was overlaid using Ub residues 2−72 in MOLMOL,[41] and the resulting ternary complex was analyzed for the presence of van der Waals clashes without any further structural refinement or use of additional experimental restraints, or allowing for any backbone or side chain flexibility. The structures were rated from "highly likely" to "highly unlikely" to form a ternary complex. In the former,

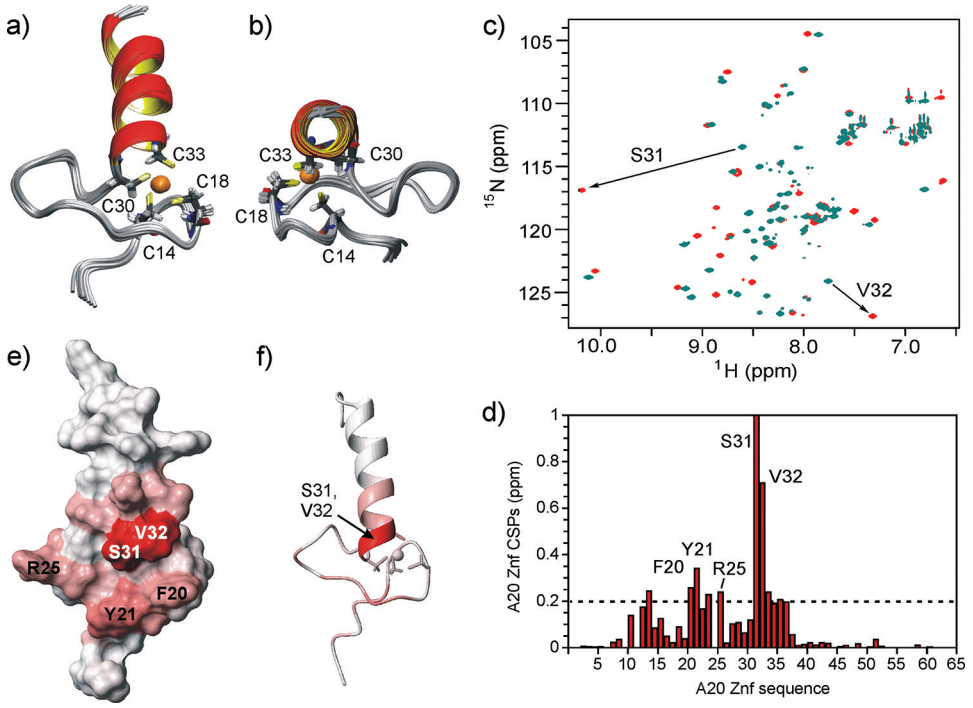

Figure 1. Ensemble of NMR structures of the A20 Znf domain of ZNF216 (residues 14−44) showing the four-Cys cluster bound to Zn^{2+} in two orientations (a and b). (c) Overlaid $^{1}H-^{15}N$ HSQC spectra (pH 7.0 at 298 K) of the free and bound states of the A20 Znf domain illustrating the highly perturbed cross-peaks for residues Ser31 and Val32. (d) Histogram of the weighted CSP data from panel b with Ser31 off-scale with a CSP of 1.7 ppm. van der Waals surface (e) and ribbon (f) representations of the A20 Znf domain with residues color-coded according to the magnitude of CSPs on binding Ub (red for the largest).

no steric clashes were identified and the two UBDs were not in close proximity to each other. In the case of likely interactions, there were similarly no steric clashes evident, but flexible loops were placed in close proximity, suggesting that contacts were possible as a consequence of local protein dynamics. In the case of unlikely interactions, direct contacts that could only in part be relieved through conformational changes within flexible loops were observed, or more severely (highly unlikely), where major van der Waals violations that could not be readily relieved without major structural reorganization were identified. The PDB coordinates used for the various UBD−Ub complexes are as follows: 2C7N for A20 Znf, 2C7N for MIU, 1Q0W for UIM, 1WR1 and 2DEN for UBA, 1OTR for CUE, 1Q5W for NZF, 1S1Q for UEV, 2Z59 for PRU, 2G45 for Znf UBP/PAZ or DUB, 2KJH for UBCH8-E3, 2DX5 for GLUE, 2K8B for PFUC, no entry for UBZ (taken from the model shown in ref 45), 1YD8 for GAT, 2KHW for UBM, 2JT4 for SH3, 2D3G for DUIM, 2FUH for UBCH5-E2, 3LDZ for VHS, and 2ZNV for MPN/JAB1-DUB. The MPN complex includes diUb, and this comparison uses the proximal Ub for only modeling.

ITC and ESI-Mass Spectrometry. Isothermal titration calorimetry (ITC) was performed on a MicroCal VP-ITC instrument. All ITC experiments were conducted in 10 mM Tris-HCl buffer (pH 7.0) 150 mM NaCl, and 50 μM $ZnCl_2$; 0.2−0.4 mM Ub was injected sequentially (5 μL) into the ITC cell (volume of 1.424 mL) containing 15−35 μM A20 Znf at 298 K. For dilution experiments, 0.2−0.5 mM A20 Znf was injected sequentially (5 μL) into the ITC cell (volume of 1.424 mL) containing only buffer (1). To investigate formation of the ternary complex, 0.3 mM A20 Znf was injected sequentially (5 μL) into the ITC cell (volume of 1.424 mL) containing 20 μM Ub or 20 μM Ub in the presence of 0.4 mM UBA at 298 K. Data were corrected using appropriate buffer and protein blanks and analyzed using MicroCal Origin to determine K_d and ΔH.

ESI-MS was performed on a Waters SYNAPT electrospray ionization, high-definition mass spectrometry (HDMS) system with a Triwave ion mobility (IM) separation cell and a quadrapole time-of-flight (qTOF) mass analyzer. Samples were injected using a mechanically driven injector and a 100 μL Hamilton syringe at a rate of 5 μL/min. Instrument control and analysis were performed in Masslynx (Waters). The total protein concentration in the range of 1−9 μM in a buffer of 25 mM ammonium acetate (pH 7) was used for all experiments. The apparent concentrations of free protein ([P]), protein·ligand complex ([PL]), and free ligand ([L]) were calculated from the concentrations of total protein and ligand used, and the signal intensities. It was assumed that P and PL gave the same, linear, detector response. Plots of [PL]/[P] versus [L] were used to determine K_d values.[46] Solvent-exposed surface areas were estimated from the average charge states of proteins in the native ESI-MS spectrum using the approach of Kaltashov and Mohimen.[47]

RESULTS

NMR Structural Analysis of the A20 Znf Domain of ZNF216. Sequence analysis of the 213-residue ZNF216 protein (rat sequence) identified an A20 Znf Ub-binding zinc finger module within the 60 N-terminal residues (Figure 1 of the Supporting Information). The structure of the A20 Znf domain was determined using multidimensional NMR methods at 600 MHz on a 1 mM sample of ^{13}C- and ^{15}N-labeled protein. NOE distance restraints, torsion angle restraints, and residual

dx.doi.org/10.1021/bi201137e | Biochemistry 2011, 50, 9076−9087

dipolar coupling (RDC) data were used to refine a family of structures using the XPLOR-NIH protocol (see Materials and Methods and Table 1).[48] A highly structured region is evident spanning residues Met12−Asn42, giving a low backbone rmsd of 0.3 Å (Figure 1a,b). A single helix extends from Cys30 to Asn42, which, although considerably shorter than that seen for Rabex-5,[9,10] is around 1.5 turns longer than other A20 Znf domain structures. Cys14 and Cys18 form a zinc knuckle with Cys30 and Cys33 located at the N-terminus of the helix completing the four-coordinate zinc cluster (Figure 1a). An 11-residue loop connects the second and third Cys residues to give a so-called treble clef zinc finger motif. The loop forms a region of stable nonregular secondary structure stabilized by a number of hydrogen bonds involving residues Met12, Cys14, Ser15, Gly17, Phe20, Gly22, Asn23, Gly28, and Met29. The overall fold of the A20 Znf domain from ZNF216 is further stabilized by contacts of both the loop and the zinc knuckle with the helix via CH−π interactions between Hβ and γMe of Thr26 in the loop and the aromatic ring of Tyr34 in the helix. The burial of Met29 against the helix and other side chains of the knuckle adds to the compact fold (Figure 2 of the Supporting Information). Alignment of the treble clef motif with other published structures (Figure 2 of the Supporting Information) shows considerable structural conservation, particularly with that of Rabex-5 (backbone rmsd around the treble clef of <0.8 Å). The ensemble of NMR structures suggests poor structural definition within the N- and C-termini, consistent with pronounced flexibility outside of the core structured region (residues 12−42).

Binding of the A20 Znf Domain of ZNF216 to Ub. The interaction of the A20 Znf domain of ZNF216 at 298 K involves a high-affinity 1:1 binding interaction with Ub [K_d = 12 ± 1.7 μM by ITC (Figure 3 of the Supporting Information)]. We mapped the two complementary binding surfaces in detail using chemical shift perturbation (CSP) methods, utilizing the sensitivity to intermolecular interactions of the ^{1}H and ^{15}N shifts in ^{1}H−^{15}N HSQC spectra. The addition of Ub to a 1 mM sample of the [^{15}N]A20 Znf domain resulted in both intermediate and slow exchange effects on line shapes. However, at molar ratios close to 1:1, and above, resonances sharpened considerably (Figure 1c). We were readily able to assign the spectra of both Ub and the A20 Znf domain in the fully bound state using different labeled proteins.

In the case of the A20 Znf domain, particularly large CSPs of 1.7 and 0.7 ppm were seen for residues Ser31 and Val32, respectively (Figure 1d), with additional significant effects (>0.2) for residues Leu13, Phe20, Tyr21, Asn23, Arg25, Cys33, and Lys35 that cluster to form a discrete binding patch involving both polar residues at the base of the helix and hydrophobic/aromatic residues from the loops of the zinc knuckle (Figure 1e,f). Analysis of the [^{15}N]Ub titration data revealed significant CSPs for residues Ile23, Asp24, and Lys48−Ser65 (Figure 2a). A cluster of highly perturbed residues (CSP > 0.35) were seen in and around the loop between β-strands 4 and 5, including Thr55, Asp58, the side chain amino group of Asn60, and Asp24 at the N-terminus of the main α-helix of Ub, presenting a small contiguous interaction surface that is largely polar in nature (Figure 2b). This contrasts with the hydrophobic β-sheet surface (centered around Ile13, Ile44, and Val70) that participates in UBA and UIM binding interactions (Figure 2c). The side chain of Asp58 sits in the center of the proposed A20 Znf binding patch, consistent with the Asp58Ala Ub mutation perturbing the interaction with

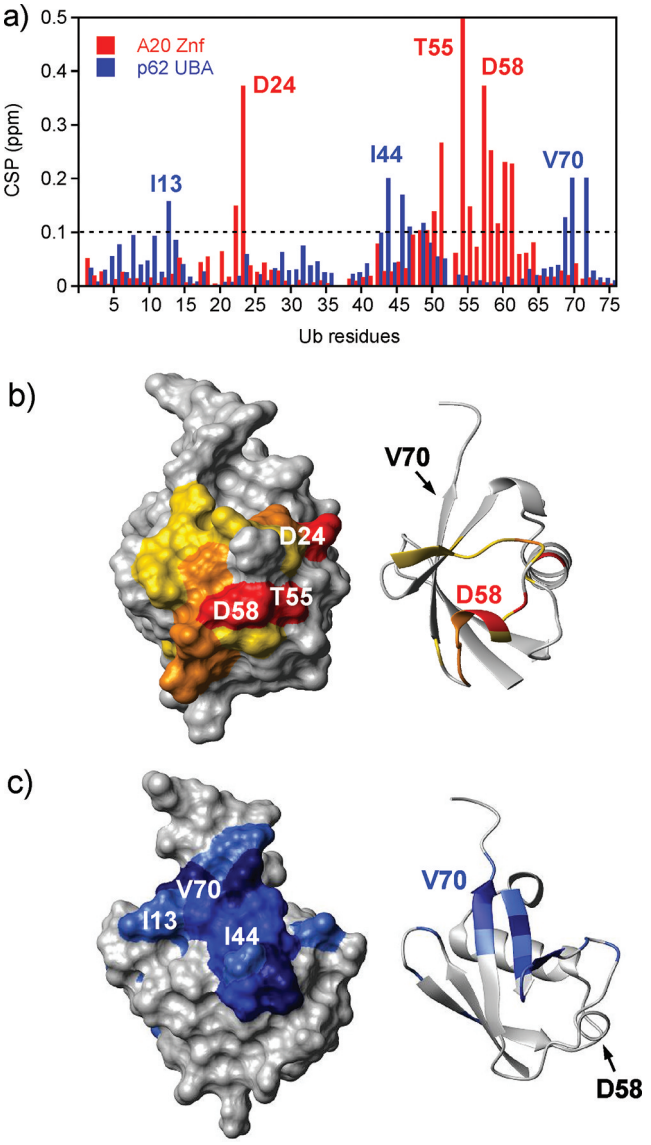

Figure 2. (a) NMR CSP data for Ub in binary complexes with A20 Znf (red) and p62 UBA domain (blue) with specific Ub residues highlighted (Thr55 off the scale at 1.23 ppm). (b) Surface and ribbon representations of Ub showing residues perturbed by the A20 Znf domain (largest effects in red). (c) Similar representations for Ub showing CSP effects from the p62 UBA domain (largest effects in dark blue).

GST−ZNF216 protein in membrane-based binding assays, but with no effects of the Ile44Ala mutation (Figure 3a).

For the purposes of structural modeling, 29 distance restraints were derived from paramagnetic relaxation enhancement (PRE) experiments (Table 2) using the MTSL spin-label covalently attached to the surface of Ub through the Lys48Cys mutation.[22,32] Complete signal attenuation was seen for residues Leu13, Cys14, Phe20, and Tyr21 in the ^{1}H−^{15}N HSQC spectrum of the A20 Znf domain, with other surrounding residues also showing significant (>85%) effects. In addition, a number of unambiguous intermolecular NOEs were identified in half-filtered NOESY experiments with a complex of [^{13}C/^{15}N]Ub with unlabeled A20 Znf, and these were combined with CSP and ^{1}H−^{15}N residual dipolar coupling (RDC) data to generate an ensemble of structures (pairwise backbone rmsd of 0.5 Å) using the molecular docking

dx.doi.org/10.1021/bi201137e | Biochemistry 2011, 50, 9076−9087

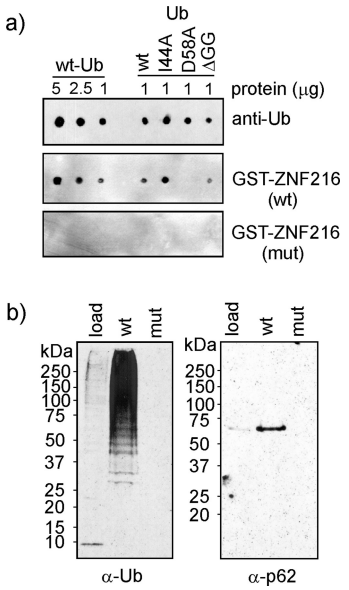

Figure 3. (a) Membrane-based binding assays demonstrating that the Asp58Ala Ub mutation, but not the Ile44Ala mutation or C-terminal Gly75/Gly76 (ΔGG) deletion, strongly perturbs the interaction with GST−ZNF216 protein (the Cys30Ala/Cys33Ala mutant GST−ZNF216 protein does not bind Ub). (b) Western blot confirming that p62 co-binds with ubiquitinated proteins from U20S cells by immobilized recombinant full-length ZNF216; the unfolded ZNF216 double mutant (Cys30Ala/Cys33Ala) was unable to capture ubiquitinated proteins or p62.

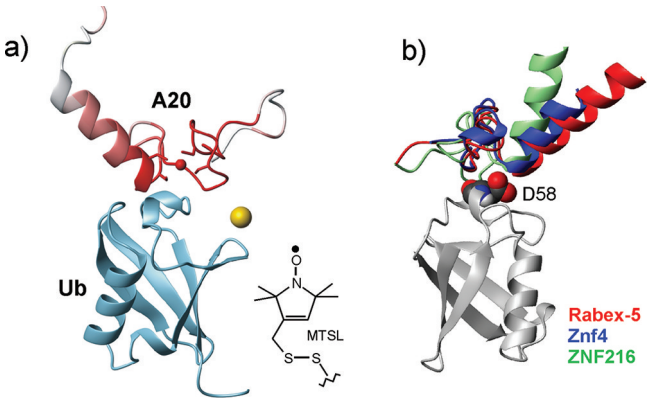

Figure 4. (a) Low-energy structure of the A20 Znf complex with Ub generated using the HADDOCK docking procedure.[42] The chemical structure of the MTSL spin-label is shown; its position covalently attached to Cys48 of Ub is represented as a yellow sphere, and the magnitude of the signal reduction in $^{1}H-^{15}N$ HSQC spectra of the complex is shaded on the A20 Znf domain, with red indicating severely attenuated. Structures were drawn using MOLMOL.[49] (b) Overlaid structures of the complexes of the A20 Znf domains of Rabex-5 (PDB entry 2FIF), Znf4 (PDB entry 3OJ3), and ZNF216 (PDB entry 2L00) on a common Ub structure showing localization around residue D58 of Ub. The extended helix of the Rabex-5 A20 Znf domain has been truncated.

program HADDOCK (see structure statistics in Table 2).[43] We further validated the structural model by substituting A20 Znf domain surface residues for those found in Rabex-5 (F20Y and V32K). Subsequent titration studies resulted in CSP effects localized to [^{15}N]Ub that were consistent with the proposed model. A low-energy structure of the complex is illustrated in Figure 4a showing the magnitude of the PRE signal attenuation on the A20 Znf domain. The structure is highly homologous to the Ub complex of the Rabex-5 A20 Znf domain and that of the second Ub (Ub2) interaction with the Znf4 A20 Ub editing protein involved in regulating cytokine-induced NF-κB signaling pathways (see overlaid structures in Figure 4b).[49] The Znf4 A20 complex is of particular note, showing the versatility of the A20 domain in interacting with three separate Ub molecules each via a unique A20 Znf interface, which together define the linkage-specific binding site for Lys63-linked triUb.[49] In the Ub complex of the A20 Znf domain of ZNF216, the formation of key hydrogen bonds between Asp58 of Ub and Ser31 of the A20 Znf domain appears to be central to the interaction along with the burial of Arg54 of Ub in the groove formed between the base of the helix and the zinc knuckle, involving Val32 and Phe20 of the A20 Znf domain (Figure 4 of the Supporting Information). Additional hydrophobic and polar contacts are made across the interface, resulting in the burial of ∼700 ± 90 Å^2 of solvent accessible surface area for the A20 Znf domain.

Modeling Multiple UBD Interactions with Ub and PolyUb Chains. ZNF216 functions in pathways related to NF-κB signaling and proteasomal proteolysis,[12,15,16] both of which are dependent on the regulation of assembly of the polyUb chain on target substrates. Substrate modification with Ub or Lys63-polyUb chains is generally associated with nondegradative processes such as NF-κB signaling, whereas non-Lys63-linked chains signal for proteosomal degradation. All of these biological pathways involve A20 Znf domain proteins (including ZNF216). We initially modeled various published diUb structures to determine the accessibility of the Asp58 Ub site for the A20 Znf domain of ZNF216 within these polyUb chains. ESI-MS confirmed that both Lys48-linked and Lys63-linked diUb are able to bind two A20 Znf domains without discrimination between chain linkages, and with affinities at each site comparable to that for binding to a single Ub (Figure 5 of the Supporting Information). We also investigated interactions of Lys63-Ub$_4$ with the A20 Znf domain by ESI-MS and could readily identify doubly and triply bound species.

The structure of the A20 Znf complex with Ub shows that the classical β-sheet hydrophobic patch around Ile44, recognized by many other UBDs, is largely unperturbed by the A20 Znf domain interaction, suggesting the possibility of Ub-mediated colocalization of other UBD-containing receptors at different surface sites. We evaluated the possibility of these UBD pairings by modeling representative members of 20 other UBD families so far characterized using UBD−Ub structures deposited in the PDB. Each structure was overlaid using Ub residues 2−72 in MOLMOL,[41] and pairwise interactions of UBD with Ub were rated from highly likely to highly unlikely to form a ternary complex on the basis of the presence or absence of steric clashes between the two UBDs (Figure 5a). As previously reported, the backbone rmsd for Ub across all 20 complexes was low (≤0.6 Å), indicating that UBD-specific conformational preferences were not a significant additional consideration.[50,51] As anticipated, the majority of UBD pairings compete for the common Ile44-centered patch; however, ∼30 pairs of UBD ternary interactions seem likely or highly likely. A number of representative structures from the different categories are highlighted in Figure 5b−d.

Interestingly, the compatibility of the pairs of interactions is not solely determined by the specific interaction site, but also by the mode of binding and the size of the UBD. The long α-helix of the MIU domain, for example, which binds on an Ile44-

dx.doi.org/10.1021/bi201137e | Biochemistry 2011, 50, 9076−9087

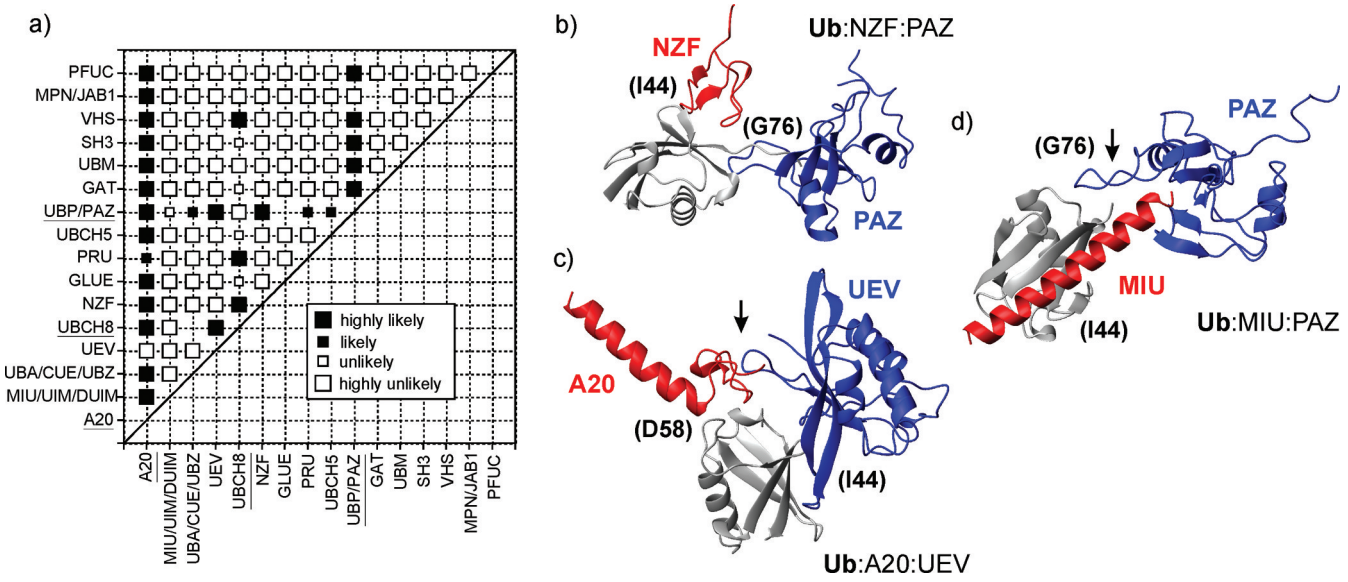

Figure 5. (a) Representation of the likelihood of pairwise interactions of all possible combinations of UBDs in putative ternary complexes with Ub. Each ternary complex was judged to be highly likely, likely, unlikely, or highly unlikely on the basis of observed steric contacts in structural models from PDB coordinates. A blank represents some ambiguity in the analysis. UBDs that are underlined do not bind through the canonical Ile44 site on Ub. The analysis assumes that for UBD families with multiple members, all members bind in a similar mode. (b–d) Molecular models of the ternary complexes of Ub with members of different UBD families. (b) NZF and PAZ are mutually compatible partners (highly likely). (c) Steric contacts between the A20 Znf domain (Rabex-5) and UEV suggest that this is not a viable ternary complex (highly unlikely). (d) In the complex of Ub with MIU and PAZ, steric contacts prevent simultaneous interactions (unlikely). Proposed steric contacts are shown with an arrow.

centered patch, causes steric clashes that appear to preclude the colocation of the PAZ domain that binds to the distant flexible C-terminal tail (Figure 5d).[4,5] Smaller Ile44 binders such as the NZF domain appear to have no such clashes (Figure 5b). In contrast, the large Ile44-binding UEV domain appears to be the only UBD unlikely to be able to pair with the A20 Znf domain despite using distinct binding patches (Figure 5c). The analysis also shows where interactions are predicted to be competitive. In a scenario where two UBDs have differing Ub binding affinities but overlapping interaction surfaces, the analysis identifies possible UBD pairs that could sequentially pass ubiquitinated cargo in a processive manner between different Ub receptors.

Evidence of Multiple Interactions of Ub with Different UBDs. The A20 Znf domain was predicted to be highly likely to form a ternary complex when a UBA domain is localized to the Ile44 hydrophobic surface of Ub (Figure 5a). Notably, ZNF216 and the UBA domain protein p62 share common functions as shuttle factors delivering ubiquitinated proteins to the 26S proteasome.[12,52] In addition, both proteins appear to be multifunctional, and separate studies have previously linked ZNF216 and p62 to the same biologically relevant TRAF6-containing signaling complex in which TRAF6 is polyubiquitinated in response to various stimuli.[16,19] We have previously studied in detail the Ub binding interaction of the p62 UBA domain.[18,21]

In addition to the existing evidence that ZNF216 and p62 function in the same biological pathway(s),[12,16,19,52] we were also able to show that the two proteins can indirectly interact in a complex mediated via polyUb. We used immobilized recombinant full-length ZNF216 to bind endogenous ubiquitinated proteins from U20S cells. A ZNF216 double mutant (Cys30Ala/Cys33Ala), defective in Ub binding,[12] was used as a control and was unable to capture ubiquitinated proteins (Figure 3b). Western blotting confirmed that endogenous p62 co-interacted with only wild-type ZNF216, indicating that a Ub-mediated interaction between the two proteins is possible. In support of this observation, we noted that in cells cotransfected with ZNF216, p62, TRAF6, and ubiquitin, wild-type ZNF216 was usually colocalized with p62-positive inclusions that also invariably contained TRAF6/ubiquitin (data not shown, consistent with refs 53 and 54) whereas mutant ZNF216 did not colocalize with p62 (Figure 6).

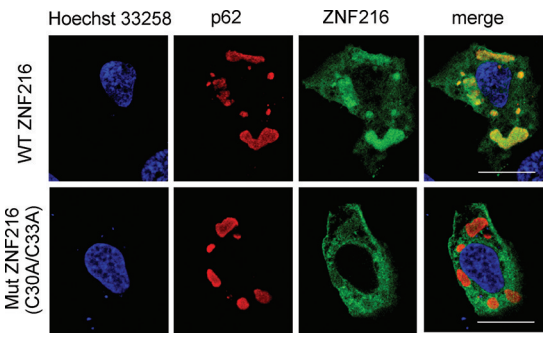

Figure 6. Indirect immunofluorescence staining and confocal microscopy images showing cells cotransfected with ZNF216, p62, TRAF6, and ubiquitin. Wild-type (WT) ZNF216 is shown to colocalize with p62-positive inclusions (merged images) that also contain TRAF6/ubiquitin (data not shown, consistent with the results of refs 53 and 54). Images for mutant ZNF216 did not show evidence of colocalization with p62.

However, these results, together with the pull-down experiments illustrated in Figure 3, do not allow us to distinguish between binding of Ub receptors to different Ub moieties in a polyUb chain and multiple-independent interactions with the same Ub. Subsequently, we investigated the interaction of Lys63-linked diUb and Ub_4 with the A20 Znf and p62 UBA domains by ESI-MS. In vitro, the ability of the

dx.doi.org/10.1021/bi201137e | *Biochemistry* 2011, 50, 9076–9087

UBA domain to form a stable homodimer significantly diminishes the effective concentration of the monomeric Ub-binding UBA domain, which also binds Ub with a 4-fold lower affinity (12 μM) than the A20 Znf domain (42 μM). Despite these affinity differences, we were able to detect a range of low-abundance species in solution (Figure 6 of the Supporting Information), including 1:2:2 and 1:3:1 Ub_4·A20·UBA ternary complexes and 1:1:1 and 1:2:1 diUb·A20·UBA ternary complexes. Although only the latter unambiguously confirms the simultaneous interaction of both the A20 Znf and UBA domain with the same Ub motif, in combination it is clear that multiple UBDs are readily accommodated on the same polyUb chain.

The NMR CSP analysis of the binary complexes of [^{15}N]Ub with the A20 Znf domain and with the p62 UBA domain suggests a degree of overlap between the two sites (Figure 2a), which may reflect induced-fit contributions to the specificity of binding UBDs to Ub,[51] demonstrating the need for further experimental validation of ternary complex formation. [^{15}N]Ub was used to monitor interactions of UBD at the two sites on a single Ub (Figure 7). Titration of the A20 Znf domain with

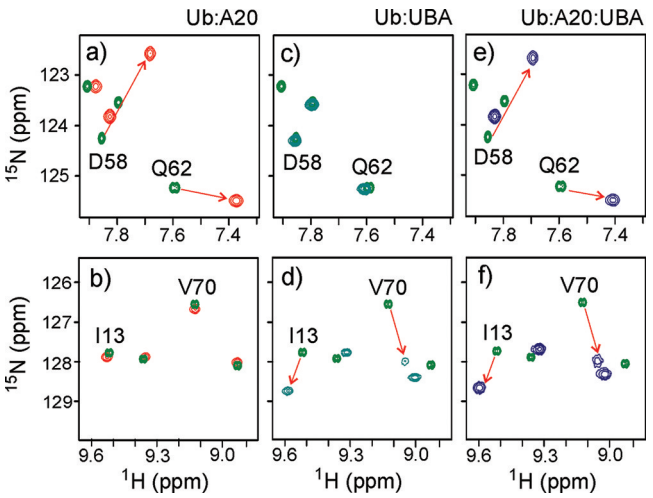

Figure 7. Portions of the ^{1}H–^{15}N HSQC spectra of Ub (pH 7.0 and 298 K) illustrating perturbations to specific residues on the different surface binding patches of Ub (arrows indicate free → bound). In the top panels (a, c, and e), the cross-peaks for Asp58 and Gln62 that form part of the A20 Znf binding surface are highlighted, and in the bottom panels (b, d, and f), residues Ile13 and Val70 within the UBA binding site are highlighted. Titration of [^{15}N]Ub with A20 Znf perturbs Asp58 and Gln62 (a), but Ile13 and Val70 are unaffected (b). Formation of the binary complex of p62 UBA with Ub leaves Asp58 and Gln62 unaffected (c), but large CSPs are evident for Ile13 and Val70 (d). In the formation of the Ub ternary complex, both sets of resonances are perturbed, demonstrating simultaneous binding of the two UBDs.

[^{15}N]Ub resulted in characteristic perturbations to Asp58 and Gln62 of Ub, but significantly no effects on Ile13 and Val70 (Figure 7a,b). In contrast, formation of a binary complex between [^{15}N]Ub and the p62 UBA leads to perturbations to the latter but not the former (Figure 7c,d). However, titration of [^{15}N]Ub with first the A20 Znf domain and then the p62 UBA domain to form the ternary complex resulted in perturbations to both sets of signals (Figure 7e,f) and well-defined surface binding patches on Ub that are well represented by the sum of the individual effects from the binary complexes of the two UBDs (Figure 8a). This was confirmed by ITC

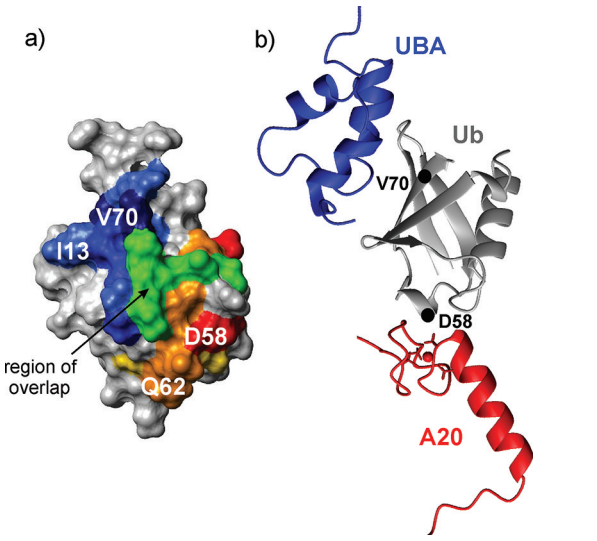

Figure 8. (a) Ub surface showing the area of potential overlap (green) between UBD sites identified from the CSP data (Figure 2a). (b) Model of the Ub·A20·UBA ternary complex generated from the overlay of the experimentally determined binary complexes. Positions of key Ub residues (D58 and V70) are highlighted.

studies at 298 K in which the A20 Znf domain was injected into Ub in both the absence and presence of 400 μM p62 UBA. The binding isotherms (Figure 3 of the Supporting Information) were fit with a K_d of 11.5 ± 1.5 μM (binary complex) or a K_d of 8.0 ± 2.5 μM (ternary complex) with 1:1 Ub–A20 binding stoichiometries (1.03 ± 0.1). Within experimental error, the binding affinity of the A20 Znf domain for Ub appears to be independent of the occupation of the UBA binding site. Moreover, HSQC spectra of ternary complexes using different combinations of ^{15}N-labeled UBDs showed no evidence of surface contacts between the two domains, consistent with the model of the complex shown in Figure 8b. Our analysis shows that a single polyUb chain is readily decorated with different UBDs and, indeed, does not preclude formation of the ternary complex either through a single Ub or through interaction with two different Ubs within the same chain.

DISCUSSION

Ub modifications are transduced by receptor proteins that recognize distinct interaction faces on the Ub surface. As is already well established, there is evidence within the UBA family of UBDs of isopeptide linkage recognition, permitting discrimination between Lys48- and Lys63-polyUb chains and signaling specificity.[55,56] Further, ternary complexes in which multiple UBL/UBD proteins bind simultaneously to the same polyUb chain have been described, resulting in altered binding affinities through colocalization effects. Both human S5a and Rad23A are involved in targeting polyubiquitinated substrates to the proteasome and can simultaneously bind to a Ub_4 chain, further facilitated by UIM and UBL interactions between the two receptors.[57] In the same context, the proteasome receptors Rpn13 and S5a have been shown to bind Lys48-diUb in concert,[58,59] with the Pru domain of Rpn13 initially displacing one of the UIMs of S5a that then competes for the other distal subunit binding site on diUb, regulating proteasomal delivery as well as deubiquitination. Formation of the ternary complex has implicated yeast proteins Dsk2 and Rpn10 in the mechanism for "counting" Ub monomers in longer chains, using a

dx.doi.org/10.1021/bi201137e | Biochemistry 2011, 50, 9076–9087

combination of UIMs and UBAs with different affinities for UBL motifs and for Ub to shift the equilibria toward different bound states in a Ub chain length-dependent manner,[60] providing a plausible mechanism for substrate release and proteasomal docking.

The effects of the wide variation in UBD binding affinities for Ub, coupled with the ability to assemble several partners on a single polyUb chain, have been highlighted as having a significant impact on mechanisms of Ub signaling and processing of ubiquitinated substrates.[7] We have extended this model to confirm that formation of the ternary complex is not limited to binding to a single polyUb chain, but an individual Ub moiety can simultaneously participate in multiple interactions with different Ub receptors in a biologically relevant context. The concept that multiple proteasome shuttle factors, such as p62 and ZNF216, can interact with the same ubiquitinated substrate, potentially affording greater specificity and affinity in delivery to the proteasome, is an attractive one. It also suggests additional mechanisms for mediating multiprotein complex assembly, or by which ubiquitinated cargo could be "handed off" from one Ub receptor protein to another.[8,61] The proposed versatility in binding the A20 domain in concert with other UBDs has recently been illustrated by formation of a complex by UbcH5A, an E2 enzyme that cooperates in polyUb chain assembly, in a Ub-mediated A20−UbcH5A interaction, potentially downregulating UbcH5A activity with inhibition of NF-κB signaling.[49] Alternatively, endocytic sorting may be a good example of sequentially passing a ubiquitinated cargo in a processive manner between different Ub receptors,[62] where the UEV domain protein (Vps23) and UIM protein (Vps27) are proposed to hand off ubiquitinated cargo by competing for common Ub-binding sites. The data in Figure 5a predict that ternary complexes involving Ub receptors are likely to be widespread in nature, as are such "hand-off" mechanisms or multivalent interactions involving individual Ub moieties.[63]

The binding of multiple UBDs to a single Ub molecule also suggests the possibility of negative regulation where certain combinations of different UBDs are not permitted. Relative affinities at overlapping sites, resulting in the competitive displacement of UBDs by tighter binding ligands, may be a further consideration in signal transduction and regulation. In the context of the endosomal trafficking complex required for transport (ESCRT) of the multivesicular body pathway, ubiquitinated cargo appears to be sorted and passed between at least three Ub-binding receptors via three sequential steps involving three UBDs (UIM, NZF, and UEV) with similar affinities.[64] A competitive displacement model is plausible, given that none of the UBDs are predicted to form viable ternary complexes because all have similar Ile44 Ub site specificities (see Figure 5a).

UBDs are typically small binding motifs, often (although not exclusively) found at the termini of larger receptors and tethered through an unstructured flexible linker. The "hook and line" architecture of these large protein receptors, including ZNF216 and p62,[65] may allow the UBD to function as a largely independent binding domain with the intrinsic flexibility facilitating the assembly of Ub-mediated ternary complexes (Figure 8b).[57−60] These conclusions demonstrate the possibility of Ub behaving as a hub for the recruitment and colocalization of receptors in multicomplex assemblies for regulating diverse intracellular molecular signaling events.

■ ASSOCIATED CONTENT

Ⓢ Supporting Information

Six figures showing the amino acid sequence alignment for A20 Znf domains, structures of the A20 Znf and its ubiquitin complex, and ITC and ESI-MS data for formation of binary and ternary complexes between ubiquitin and the ZNF216 A20 Znf domain and p62 UBA domain. This material is available free of charge via the Internet at http://pubs.acs.org.

Accession Codes

Coordinates and structural details for the A20 Znf domain and its binary complex with ubiquitin were deposited in the Protein Data Bank as entries 2KZY and 2L00, respectively. The corresponding NMR data were deposited at the BMRB as entries 17023 and 17024.

■ AUTHOR INFORMATION

Corresponding Author

*Centre for Biomolecular Sciences, School of Chemistry, University Park, University of Nottingham, Nottingham NG7 2RD, U.K. E-mail: mark.searle@nottingham.ac.uk. Telephone: (44) 0115 951 3567.

Funding

We thank the EPSRC and BBSRC of the United Kingdom for providing funding and the University of Nottingham for support for core instrumentation.

■ ACKNOWLEDGMENTS

We thank Dr. Huw Williams for technical support with NMR experiments and structural modeling, Dr. David Scott for running AUC experiments, and Drs. Simon Dawson and Paul Evans (School of Biomedical Sciences, University of Nottingham) for kindly providing plasmids.

■ ABBREVIATIONS

Ub, ubiquitin; polyUb, polyubiquitin; Znf, zinc finger; UBD, ubiquitin binding domain; UBA, ubiquitin-associated domain; NMR, nuclear magnetic resonance; ITC, isothermal titration calorimetry; CSP, chemical shift perturbation; ESI-MS, electrospray ionization mass spectrometry; rmsd, root-mean-square deviation.

■ REFERENCES

(1) Komander, D. (2009) The emerging complexity of protein ubiquitination. *Biochem. Soc. Trans. 37*, 937−953.

(2) Seet, B. T., Dikic, I., Zhou, M. M., and Pawson, T. (2006) Reading protein modifications with interaction domains. *Nat. Rev. Mol. Cell Biol. 7*, 473−483.

(3) Hagai, T., and Levy, Y. (2010) Ubiquitin not only serves as a tag but also assists degradation by inducing protein unfolding. *Proc. Natl. Acad. Sci. U.S.A. 107*, 2001−2006.

(4) Dikic, I., Wakatsuki, S., and Walters, K. J. (2009) Ubiquitin-binding domains: From structures to functions. *Nat. Rev. Mol. Cell Biol. 10*, 659−671.

(5) Harper, J. W., and Schulman, B. A. (2006) Structural complexity in ubiquitin recognition. *Cell 124*, 1133−1136.

(6) Bomar, M. G., D'Souza, S., Bienko, M., Dikic, I., Walker, G. C., and Zhou, P. (2010) Unconventional ubiquitin recognition by the ubiquitin-binding motif within the Y family DNA polymerases ι and Rev1. *Mol. Cell 37*, 408−417.

(7) Winget, J. M., and Mayor, T. (2010) The diversity of ubiquitin recognition: Hot spots and varied specificity. *Mol. Cell 38*, 627−635.

(8) Chen, Z. J., and Sun, L. J. (2009) Nonproteolytic functions of ubiquitin in cell signaling. *Mol. Cell 33*, 275−286.

(9) Lee, S., Tsai, Y. C., Mattera, R., Smith, W. J., Kostelansky, M. S., Weissman, A. M., Bonifacino, J. S., and Hurley, J. H. (2006) Structural basis for ubiquitin recognition and autoubiquitination by Rabex-5. *Nat. Struct. Mol. Biol. 13*, 264−271.

(10) Penengo, L., Mapelli, M., Murachelli, A. G., Confalonieri, S., Magri, L., Musacchio, A., Di Fiore, P. P., Polo, S., and Schneider, T. R. (2006) Crystal structure of the ubiquitin binding domains of Rabex-5 reveals two modes of interaction with ubiquitin. *Cell 124*, 1183−1195.

(11) Sato, Y., Yoshikawa, A., Yamagata, A., Mimura, H., Yamashita, M., Ookata, K., Nureki, O., Iwai, K., Komada, M., and Fukai, S. (2008) Structural basis for specific cleavage of Lys 63-linked polyubiquitin chains. *Nature 455*, 358−362.

(12) Hishiya, A., Iemura, S., Natsume, T., Takayama, S., Ikeda, K., and Watanabe, K. (2006) A novel ubiquitin-binding protein ZNF216 functioning in muscle atrophy. *EMBO J. 25*, 554−564.

(13) Lecker, S. H., Solomon, V., Mitch, W. E., and Goldberg, A. L. (1999) Muscle protein breakdown and the critical role of the ubiquitin-proteasome pathway in normal and disease states. *J. Nutr. 129*, 227S−237S.

(14) Murton, A. J., Constantin, D., and Greenhaff, P. L. (2008) The involvement of the ubiquitin proteasome system in human skeletal muscle remodelling and atrophy. *Biochim. Biophys. Acta 1782*, 730−743.

(15) Hishiya, A., Ikeda, K., and Watanabe, K. (2005) A RANKL-inducible gene Znf216 in osteoclast differentiation. *J. Recept. Signal Transduction Res. 25*, 199−216.

(16) Huang, J., Teng, L., Li, L., Liu, T., Li, L., Chen, D., Xu, L. G., Zhai, Z., and Shu, H. B. (2004) ZNF216 Is an A20-like and IκB kinase γ-interacting inhibitor of NF-κB activation. *J. Biol. Chem. 279*, 16847−16853.

(17) Chen, Z. J. (2005) Ubiquitin signalling in the NF-κB pathway. *Nat. Cell Biol. 7*, 758−765.

(18) Long, J., Garner, T. P., Pandya, M. J., Craven, C. J., Chen, P., Shaw, B., Williamson, M. P., Layfield, R., and Searle, M. S. (2010) Dimerisation of the UBA Domain of p62 Inhibits Ubiquitin Binding and Regulates NF-κB Signalling. *J. Mol. Biol. 396*, 178−194.

(19) Sanz, L., Diaz-Meco, M. T., Nakano, H., and Moscat, J. (2000) The atypical PKC-interacting protein p62 channels NF-κB activation by the IL-1-TRAF6 pathway. *EMBO J. 19*, 1576−1586.

(20) Sanz, L., Sanchez, P., Lallena, M. J., Diaz-Meco, M. T., and Moscat, J. (1999) The interaction of p62 with RIP links the atypical PKCs to NF-κB activation. *EMBO J. 18*, 3044−3053.

(21) Long, J., Gallagher, T. R., Cavey, J. R., Sheppard, P. W., Ralston, S. H., Layfield, R., and Searle, M. S. (2008) Ubiquitin recognition by the ubiquitin-associated domain of p62 involves a novel conformational switch. *J. Biol. Chem. 283*, 5427−5440.

(22) Zhang, D., Raasi, S., and Fushman, D. (2008) Affinity makes the difference: Nonselective interaction of the UBA domain of Ubiquilin-1 with monomeric ubiquitin and polyubiquitin chains. *J. Mol. Biol. 377*, 162−180.

(23) Thompson, J. D., Gibson, T. J., Plewniak, F., Jeanmougin, F., and Higgins, D. G. (1997) The CLUSTAL X windows interface: Flexible strategies for multiple sequence alignment. *Nucleic Acids Res. 25*, 4876−4882.

(24) The UniProt Consortium (2009) The Universal Protein Resource (UniProt). *Nucleic Acids Res. 37*, D169−D174.

(25) Schultz, J., Milpetz, F., Bork, P., and Ponting, C. P. (1998) SMART, a simple modular architecture research tool: Identification of signalling domains. *Proc. Natl. Acad. Sci. U.S.A. 95*, 5857−5864.

(26) Gould, C. M., Diella, F., Via, A., Puntervoll, P., Gemund, C., Chabanis-Davidson, S., Michael, S., Sayadi, A., Bryne, J. C., Chica, C., Seiler, M., Davey, N. E., Haslam, N., Weatheritt, R. J., Budd, A., Hughes, T., Pas, J., Rychlewski, L., Trave, G., Aasland, R., Helmer-Citterich, M., Linding, R., and Gibson, T. J. (2010) ELM: The status of the 2010 eukaryotic linear motif resource. *Nucleic Acids Res. 38*, D167−D180.

(27) Vranken, W. F., Boucher, W., Stevens, T. J., Fogh, R. H., Pajon, A., Llinas, P., Ulrich, E. L., Markley, J. L., Ionides, J., and Laue, E. D. (2005) The CCPN data model for NMR spectroscopy: Development of a software pipeline. *Proteins: Struct., Funct., Bioinf. 59*, 687−696.

(28) Ottiger, M., Delaglio, F., and Bax, A. (1998) Measurement of J and dipolar couplings from simplified two-dimensional NMR spectra. *J. Magn. Reson. 131*, 373−378.

(29) Chou, J. J., Gaemers, S., Howder, B., Louis, J. M., and Bax, A. (2001) A simple apparatus for generating stretched polyacrylamide gels, yielding uniform alignment of proteins and detergent micelles. *J. Biomol. NMR 21*, 377−382.

(30) Kay, L. E., Torchia, D. A., and Bax, A. (1989) Backbone dynamics of proteins as studied by ^{15}N inverse detected heteronuclear NMR spectroscopy: Application to staphylococcal nuclease. *Biochemistry 28*, 8972−8979.

(31) Otting, G., and Wuthrich, K. (1989) Extended heteronuclear editing of 2D ^{1}H-NMR spectra of isotope-labelled proteins using the X(ω1,ω2) double half-filter. *J. Magn. Reson. 85*, 586−594.

(32) Liang, B., Bushweller, J. H., and Tamm, L. K. (2006) Site-directed parallel spin-labeling and paramagnetic relaxation enhancement in structure determination of membrane proteins by solution NMR spectroscopy. *J. Am. Chem. Soc. 128*, 4389−4397.

(33) Wu, Y., Shih, S. C., and Goto, N. K. (2007) Probing the structure of the Ff bacteriophage major coat protein transmembrane helix dimer by solution NMR. *Biochim. Biophys. Acta 1768*, 3206−3215.

(34) Berjanskii, M. V., and Wishart, D. S. (2007) The RCI server: Rapid and accurate calculation of protein flexibility using chemical shifts. *Nucleic Acids Res. 35*, W531−W537.

(35) Sass, H. J., Musco, G., Stahl, S. J., Wingfield, P. T., and Grzesiek, S. (2001) A easy way to include weak alignment constraints into NMR structure calculations. *J. Biomol. NMR 21*, 275−280.

(36) Dosset, P., Hus, J. C., Marion, D., and Blackledge, M. (2001) A novel interactive tool for rigid body modelling of multi-domain macromolecules using residual dipolar couplings. *J. Biomol. NMR 20*, 223−231.

(37) Schwieters, C. D., Kuszewski, J. J., Tjandra, N., and Clore, G. M. (2003) The Xplor-NIH NMR molecular structure determination package. *J. Magn. Reson. 160*, 65−73.

(38) Nilges, M., Clore, G. M., and Gronenborn, A. M. (1988) Determination of three-dimensional structures of proteins from interproton distance data by dynamical simulated annealing from a random array of atoms circumventing problems associated with folding. *FEBS Lett. 239*, 129−136.

(39) Nilges, M., Gronenborn, A. M., Brunger, A. T., and Clore, G. M. (1988) Determination of three-dimensional structures of proteins by simulated annealing with interproton distance restraints. Application to crambin, potato carboxypeptidase inhibitor and barley serine proteinase inhibitor 2. *Protein Eng. 2*, 27−38.

(40) Bhattacharya, A., Tejero, R., and Montelione, G. T. (2007) Evaluating protein structures determined by structural genomics consortia. *Proteins 66*, 778−795.

(41) Koradi, R., Billeter, M., and Wuthrich, K. (1996) MOLMOL: A program for display and analysis of macromolecular structures. *J. Mol. Graphics 14*, 51−55.

(42) Wishart, D. S., Arndt, D., Berjanskii, M., Tang, P., Zhou, J., and Lin, G. (2008) CS23D: A web server for rapid protein structure generation using NMR chemical shifts and sequence data. *Nucleic Acids Res. 36*, W496−W502.

(43) Dominguez, C., Boelens, R., and Bonvin, A. M. (2003) HADDOCK: A protein-protein docking approach based on biochemical or biophysical information. *J. Am. Chem. Soc. 125*, 1731−1737.

(44) Hubbard, S. J., and Thornton, J. M. (1993) *NACCESS*, University College London, London.

(45) Bomar, M. G., Pai, M. T., Tzeng, S. R., Li, S. S., and Zhou, P. (2007) Structure of the ubiquitin-binding zinc finger domain of human DNA Y-polymerase η. *EMBO Rep. 8*, 247−251.

(46) Veros, C. T., and Oldham, N. J. (2007) Quantitative determination of lysozyme-ligand binding in solution and gas phases

by electrospray ionisation mass spectrometry. *Rapid Commun. Mass Spectrom. 21*, 3505−3510.
(47) Kaltashov, I. A., and Mohimen, A. (2005) Estimates of protein surface areas in solution by electrospray ionisation mass spectrometry. *Anal. Chem. 77*, 5370−5379.
(48) Schwieters, C. D., Kuszewski, J. J., Tjandra, N., and Clore, G. M. (2003) The Xplor-NIH NMR molecular structure determination package. *J. Magn. Reson. 160*, 65−73.
(49) Bosanac, I., Wertz, I. E., Pan, B., Yu, C., Kusam, S., Lam, C., Phu, L., Phung, Q., Maurer, B., Arnott, D., Kirkpatrick, D. S., Dixit, V. M., and Hymowitz, S. G. (2010) Ubiquitin binding to A20 ZnF4 is required for modulation of NF-kB signalling. *Mol. Cell 40*, 548−557.
(50) Lange, O. F., Lakomek, N. A., Fares, C., Schroder, G. F., Walter, K. F., Becker, S., Meiler, J., Grubmuller, H., Griesinger, C., and de Groot, B. L. (2008) Recognition dynamics up to microseconds revealed from an RDC-derived ubiquitin ensemble in solution. *Science 320*, 1471−1475.
(51) Włodarski, T., and Zagrovic, B. (2009) Conformational selection and induced fit mechanism underlie specificity in non-covalent interactions with ubiquitin. *Proc. Natl. Acad. Sci. U.S.A. 106*, 19346−19351.
(52) Seibenhener, M. L., Geetha, T., and Wooten, M. W. (2007) Sequestosome 1/p62: More than just a scaffold. *FEBS Lett. 581*, 175−179.
(53) Siebenhener, M. L., Babu, J. R., Geetha, T., Wong, H. C., Krishna, N. R., and Wooten, M. W. (2004) Sequestome 1/p62 is a polyubiquiyin chain binding protein involved in ubiquitin proteasome degradation. *Mol. Cell. Biol. 24*, 8055−8068.
(54) Yip, K. H. M., Feng, H., Pavlos, N. J., Zheng, M. H., and Xu, J. (2006) p62 ubiquitin binding-associated domain mediated the receptor activator of nuclear factor-κB ligand-induced osteoclast formation: A new insight into the pathogenesis of Paget's disease of bone. *Am. J. Pathol. 169*, 503−514.
(55) Varadan, R., Assfalg, M., Raasi, S., Pickart, C., and Fushman, D. (2005) Structural determinants for selective recognition of a Lys48-linked polyubiquitin chain by a UBA domain. *Mol. Cell 18*, 687−698.
(56) Trempe, J. F., Brown, N. R., Lowe, E. D., Gordon, C., Campbell, I. D., Noble, M. E., and Endicott, J. A. (2005) Mechanism of Lys48-linked polyubiquitin chain recognition by the Mud1 UBA domain. *EMBO J. 24*, 3178−3189.
(57) Kang, Y., Chen, X., Lary, J. W., Cole, J. L., and Walters, K. J. (2007) Defining how ubiquitin receptors hHR23A and S5a bind polyubiquitin. *J. Mol. Biol. 369*, 168−176.
(58) Zhang, D., Wang, Q., Ehlinger, A., Randles, L., Lary, J. W., Kang, Y., Haririnia, A., Storaska, A. J., Cole, J. L., Fushman, D., and Walters, K. J. (2009) Structure of the S5a:K48-linked diubiquitin complex and its interaction with Rpn13. *Mol. Cell 35*, 280−290.
(59) Schreiner, P., Chen, X., Husnjak, K., Randles, L., Zhang, N., Elsasser, S., Finley, D., Dikic, I., Walters, K. J., and Groll, M. (2008) Ubiquitin docking at the proteosome through a novel pleckstrin-homology domain interaction. *Nature 453*, 548−552.
(60) Zhang, D., Chen, T., Ziv, I., Rosenzweig, R., Matiuhin, Y., Bronner, V., Glickman, M. H., and Fushman, D. (2009) Together, Rpn10 and Dsk2 cab serve as a polyubiquitin chain-length sensor. *Mol. Cell 36*, 1018−1033.
(61) Raiborg, C., and Stenmark, H. (2009) The ESCRT machinery in endosomal sorting of ubiquitylated membrane proteins. *Nature 458*, 445−452.
(62) Teo, H., Veprintsev, D. B., and Williams, R. L. (2004) Structural insights into endosomal sorting complex required for transport (ESCRT-I) recognition of ubiquitin proteins. *J. Biol. Chem. 279*, 28689−28696.
(63) Woelk, T., Sigismund, S., Penengo, L., and Polo, S. (2007) The ubiquitination code: A signalling problem. *Cell Div. 2*, 11−16.
(64) Hierro, A., Sun, J., Rusnak, A. S., Kim, J., Prag, G., Emr, S. D., and Hurley, J. H. (2004) Structure of the ESCRT-II endosomal trafficking complex. *Nature 431*, 221−225.
(65) Najat, D., Garner, T., Hagen, T., Shaw, B., Sheppard, P. W., Falchetti, A., Marini, F., Brandi, M. L., Long, J. E., Cavey, J. R., Searle, M. S., and Layfield, R. (2009) Characterization of a non-UBA domain missense mutation of sequestosome 1 (SQSTM1) in Paget's disease of bone. *J. Bone Miner. Res. 24*, 632−642.